Journal of Magnetic Resonance 195 (2008) 232–237

Contents lists available at ScienceDirect

Journal of Magnetic Resonance

journal homepage: www.elsevier.com/locate/jmr

Communication

Hyperpolarized ^{83}Kr MRI of lungs

Zackary I. Cleveland [a,1], Galina E. Pavlovskaya [a], Nancy D. Elkins [b], Karl F. Stupic [a], John E. Repine [b], Thomas Meersmann [a,*]

[a] Department of Chemistry, Colorado State University, Fort Collins, CO 80523, USA
[b] Webb-Waring Institute for Cancer, Aging and Antioxidant Research, University of Colorado Health Science Center, Denver, CO 80262, USA

ARTICLE INFO

Article history:
Received 21 February 2008
Revised 5 September 2008
Available online 26 September 2008

Keywords:
Laser polarized
Spin exchange optical pumping
Pulmonary disease
Alveolar surface
Lung injury

ABSTRACT

Hyperpolarized (hp) ^{83}Kr (spin $I = 9/2$) is a promising gas-phase contrast agent that displays sensitivity to the surface chemistry, surface-to-volume ratio, and surface temperature of the surrounding environment. This proof-of-principle study demonstrates the feasibility of *ex vivo* hp ^{83}Kr magnetic resonance imaging (MRI) of lungs using natural abundance krypton gas (11.5% ^{83}Kr) and excised, but otherwise intact, rat lungs located within a custom designed ventilation chamber. Experiments comparing the ^{83}Kr MR signal intensity from lungs to that arising from a balloon with no internal structure inflated to the same volume with krypton gas mixture suggest that most of the observed signal originated from the alveoli and not merely the conducting airways. The ^{83}Kr longitudinal relaxation times in the rat lungs ranged from 0.7 to 3.7 s but were reproducible for a given lung. Although the source of these variations was not explored in this work, hp ^{83}Kr T_1 differences may ultimately lead to a novel form of MRI contrast in lungs. The currently obtained 1200-fold signal enhancement for hp ^{83}Kr at 9.4 T field strength is found to be 180 times below the theoretical upper limit.

1. Introduction

Hyperpolarized (hp) noble gases [1,2] display dramatically increased signal intensities in nuclear magnetic resonance (NMR) spectroscopy and magnetic resonance imaging (MRI) enabling a wide range of novel applications [3–5]. Biomedical interest in hp gases began in the mid-1990s with proof-of-principle reports of hp ^{129}Xe [6] and hp ^{3}He [7] lung MRI. Hp ^{3}He has proven particularly valuable for studying lung ventilation distribution [8], alveolar size [9,10], and O_2 partial pressure [11]. Recently, pulmonary ^{3}He MRI was also demonstrated in very weak magnetic fields that produced ^{3}He resonance frequencies of around 200 kHz [12]. Hp ^{129}Xe yields lower signal intensities than hp ^{3}He due to its lower gyromagnetic ratio and generally lower polarization, but through its high tissue solubility and 300 ppm chemical shift range [3] provides additional information about structure and gas exchange in lungs [13–15], displays tissue-specific chemical shifts [16] and, in conjunction with functionalized xenon biosensors, can be used for molecular imaging [17,18].

However, neither hp ^{3}He, hp ^{129}Xe, nor alternative techniques using thermally polarized fluorinated gas species [19,20] can deliver information about lung surface chemistry, which is intimately linked to certain lung diseases. For instance, acute lung injury (ALI), including its most severe form acute respiratory distress syndrome (ARDS) [21], is characterized by changes in the lipid and protein composition of the pulmonary surfactant system. Additionally, disease inducing aerosols such as tobacco smoke and mineral dusts can both transiently and chronically alter the lung surface chemistry [22,23]. The current lack of available imaging technologies that allow the early diagnosis of lung surface related pathologies is the driving force to develop non-invasive, spatially resolved techniques that provide information about pulmonary surface chemistry.

Recently, the development of hp ^{83}Kr NMR and MRI was reported [24,25]. Like ^{129}Xe and ^{3}He (both nuclear spin $I = 1/2$), ^{83}Kr ($I = 9/2$) can be hyperpolarized by spin exchange optical pumping (SEOP) [26,27], and its relatively long gas-phase T_1 of up to several hundred seconds at atmospheric pressure [28,29] allows the gas to be separated from the reactive alkali metal vapor without extensive depolarization [24]. Unlike hp ^{129}Xe or ^{3}He, hp ^{83}Kr has been shown to provide MRI contrast that is highly sensitive to the surface chemistry in relatively low surface-to-volume ratio environments [30,31]. Additionally, the longitudinal relaxation of hp ^{83}Kr provides information about surface properties including surface-to-volume ratio [30], surface hydration [32], and surface temperature [24]. This sensitivity is caused by quadrupolar interactions that strongly influence the longitudinal relaxation rate when krypton is in contact with surfaces.

For instance, the T_1 of hp ^{83}Kr was shown to increase by up to a factor of twenty if tobacco smoke condensate, which contains

* Corresponding author. Fax: +1 970 491 1763.
E-mail address: Meer@MagneticResonance.US (T. Meersmann).
[1] Present address: Center for In Vivo Microscopy, Duke University Medical Center, Durham, NC 27710, USA.

1090-7807/$ - see front matter © 2008 Elsevier Inc. All rights reserved.
doi:10.1016/j.jmr.2008.09.020

numerous hydrophobic constituents [22], was deposited on model surfaces [31]. These large relaxational differences enabled T_1 contrast-weighted variable flip angle FLASH MR imaging [33] that provided spatially resolved information about both the location and amount of tobacco smoke deposited on surfaces. The sensitivity hp ^{83}Kr displays to surface-to-volume ratio within porous materials may also be of diagnostic value. Increased alveolar size due to both natural aging [10] and chronic obstructive pulmonary disease (COPD) progression [20] has been observed using hp ^{3}He apparent diffusion coefficient (ADC) measurements, while other disorders, such as ALI, are associated with alveolar collapse and thus increased surface-to-volume ratios.

Although hp ^{83}Kr has been explored as a surface sensitive contrast agent in model systems, the feasibility of hp ^{83}Kr lung MRI must still be demonstrated. Fast T_1 relaxation during inhalation and when inside the alveolar regions could potentially depolarize hp ^{83}Kr to unobservable levels. Previous studies with desiccated canine lung tissue showed promising T_1 times of about 10 s [25], but the surface chemistry and microscopic surface morphology found *in vivo* will be substantially different than those of desiccated tissue. Also, these earlier experiments were performed by rapidly shuttling hp ^{83}Kr into a pre-evacuated sample to reduce T_1 relaxation during transfer, but this technique is obviously unsuitable for *in vivo* work or *ex vivo* studies of intact lungs. In this work, we report the first hp ^{83}Kr NMR spectra, T_1 data, and hp ^{83}Kr MRI from freshly excised, but otherwise intact, rat lungs obtained with natural abundance krypton gas (11.5% ^{83}Kr) using a novel device for ventilating excised lungs. Additionally, a discussion of the maximum future improvements to the hp ^{83}Kr signal intensity is presented.

2. Materials and methods

2.1. NMR spectroscopy and MR imaging

Experiments were performed on a Chemagnetics CMX II 400 MHz NMR spectrometer in a 9.4 T, wide-bore (89 mm) superconducting magnet equipped with an imaging system (Resonance Research, Billerica, MA) consisting of triple axis gradient coils (100 G/cm *x*, y axes and 720 G/cm *z* axis) and low-noise linear gradient amplifiers. Spectra and images were obtained using a custom-built probe with a single saddle coil for excitation and detection tuned to the 15.4 MHz ^{83}Kr resonance frequency. A 15 min SEOP period was applied between consecutive hp gas deliveries to replenish the non-equilibrium ^{83}Kr polarization.

The T_1 values reported in this work were calculated by nonlinear least-squares fitting of the hp ^{83}Kr signal as a function of time, and corrected for the number of (24°) RF observation pulses. The image was produced from a series of 16 traces acquired using a non-selective, gradient–echo sequence with phase encoding gradients incremented in each hp gas delivery. To reconstruct the image, acquisition matrices were zero-filled to 32 points in both dimensions and apodized using a sine bell squared function before Fourier transformation in each dimension. Image processing was performed in MATLAB R2006a (Version 14.2; Math-works, Natick, MA).

2.2. Spin exchange optical pumping

SEOP of ^{83}Kr [1] was performed in untreated, cylindrical Pyrex cells (length = 125 mm, ID = 24 mm) as previously described [24]. The krypton mixture was produced from research grade gases (Airgas, Radnor, PA) and contained 25% krypton (natural abundance, 99.995% pure), 5% N_2 (99.9997% pure), and 70% helium (99.9999% pure). Pump cells containing ~1 g of rubidium (99.75%; Alfa Aesar, Ward Hill, MA) were housed in a quartz and aluminum oven to maintain even heating (438 ± 5 K) and maintained above ambient pressure (~120 kPa) to avoid atmospheric contamination. Light (794.7 nm) from two 30 W Coherent FAP diode-array lasers (line width ~2 nm) was directed via fiber optic coupling cables through a circular polarizer onto the pump cell. SEOP occurred in the fringe field of the superconducting magnet at approximately 0.05 T using a 'stopped flow mode' where the gas flow was stopped for 15 min. The rubidium vapor was then separated from the hp gas mixtures by an air-cooled trap at the outlet of the pump cell, and the hp ^{83}Kr gas was then transferred into the lungs as described in Section 2.4.

2.3. Animal care and usage

The Institutional Animal Care and Use Committee of the University of Colorado at Denver and Health Sciences Center approved the protocol used in this work. Seven healthy, male Sprague–Dawley rats (Charles River Laboratories, Inc., Wilmington, MA) were acclimated to altitude (~1600 m) for at least 14 days while being fed a normal diet and weighed 193–266 g at the time of lung excision. The rats were anesthetized with ketamine (80 mg/kg) and xylazine (16 mg/kg) (MWT Veterinary Supply) delivered intraperitoneally. The trachea was clamped at time of inhalation to avoid collapsing the airways while removing the heart and lungs from chest cavity. The right ventricle was injected with 100 USP units heparin (American Pharmaceutical Partners, Inc., Schaumburg, IL) and allowed to circulate for 10–15 s before the heart and lungs were excised *en bloc*. The trachea was then cannulated with an indwelling 16-gauge stub adapter tube positioned 5 mm above the bifurcation of the lungs.

2.4. Lung ventilation

Following excision, the lungs, with the heart still attached, were placed in a Pyrex ventilation chamber (ID = 24 mm and height = 100 mm; see Fig. 1a) and immersed in isotonic saline solution (0.9% NaCl, pH 5.5; Baxter Heathcare Corporation, Deerfield, IL). The lungs were then inflated with 4–5 ml of air and transported at 277 K to the imaging facility. To prevent flooding of the airways and hp ^{83}Kr from escaping before entering the lung, the trachea was tightly sutured to the stub adapter tube affixed to the bottom of the inflation chamber. Upon inflation, experiments were performed only if no gas bubbling was observed either at the location of the sutures or from the lungs themselves indicating that the gas entered and remained within the lungs. Consequently, three of the seven sets of lungs were not used for experiments.

Hp ^{83}Kr needed to reach the lungs quickly enough to avoid substantial T_1 relaxation during transfer while maintaining at most a slight overpressure to prevent lung damage. Therefore, the hp ^{83}Kr was transferred (see Fig. 1b) after 15 min of SEOP by pressure equalization from the SEOP cell to a pre-evacuated (pressure <10 Pa) Pyrex storage cell (length = 80 mm, ID = 24 mm). After the pressure equalized, the valve separating the storage cell from the Pyrex transfer tubing was opened, and the hp gas flowed from the storage cell through the inner tube (ID = 2 mm) and past the entrance of the lung. The lungs were inflated by applying a slight suction above the saline solution and deflated by applying a slight overpressure. In doing so, the lungs were ventilated with 6 ml of hp gas, as monitored by saline solution displacement. Although the presence of a breathable concentration of paramagnetic oxygen was previously shown to lower the T_1 of ^{83}Kr by only about 20% [25], it, along with other gases [29] could introduced variability to the observed relaxation. Therefore, prior to experiments, the lungs were repeatedly ventilated with nitrogen gas to remove residual air and thus provide consistent initial conditions for the

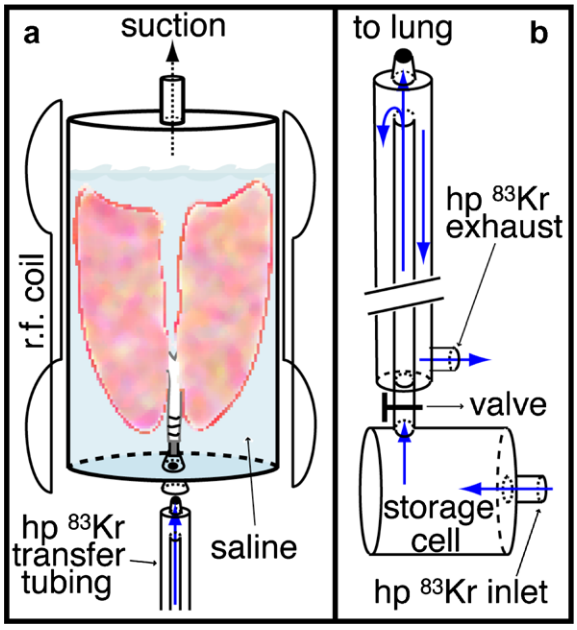

Fig. 1. Apparatus for delivering hp ^{83}Kr to lungs. The thick, solid arrows indicate the direction of hp ^{83}Kr flow. (a) *Ex vivo* lung ventilation chamber. The lungs were inverted (trachea pointing down) and completely immersed in a physiological saline solution. The lungs were then inflated with 6 ml of hp gas mixture by applying a slight suction and deflated by applying slight overpressure. Hp ^{83}Kr flowed past the entrance to the lungs and was pulled into the lungs during inflation. (b) Hp ^{83}Kr transfer system. The storage cell was evacuated to less than 10 Pa, and hp ^{83}Kr was transferred from the SEOP cell by pressure equalization (final pressure ~110 kPa). The valve was then opened, and gas flowed from the storage cell, through the inner tube, and past the entrance to the lung. Hp ^{83}Kr was either pulled into the lung during inflation or flowed through the outer tube to the ambient air.

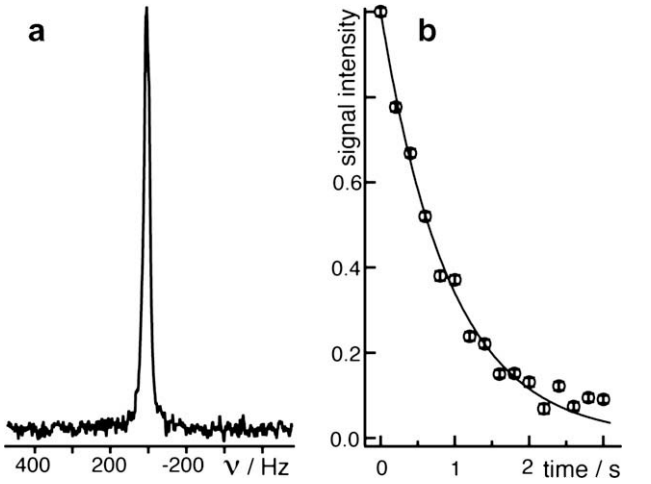

Fig. 2. Hp ^{83}Kr NMR spectroscopy. (a) Typical hp ^{83}Kr spectrum from excised rat lungs at 9.4 T. (b) Signal intensity decay curve of hp ^{83}Kr in rat lungs resulting from both longitudinal relaxation and RF. Data points are signal intensities of the hp ^{83}Kr spectra obtained from a series of 24° RF pulses normalized to the signal intensity resulting from the first pulse. The error bars are the standard deviations in the baseline noise.

experiments described in this work. Further, the flow of the hp gas past the lungs was monitored by a flow meter located at the exit of the hp-gas transfer system into the ambient air to assure that no backflow took place during the inhalation procedure.

3. Results and discussion

3.1. Spectroscopy and MR imaging of lungs

Fig. 2a displays a representative hp ^{83}Kr NMR spectrum from excised rat lungs following a 90° RF pulse. The highest hp ^{83}Kr signal intensities that were previously obtained from the 25% krypton mixture used in this work were enhanced approximately 4500 times over that of thermally polarized krypton at 9.4 T. This enhancement corresponded to a spin polarization of about 1% [32]. However, this intensity was only observed by vacuum shuttling hp ^{83}Kr into the detection region. The signal enhancement from lungs in the current work was probably reduced about 50% by relaxation during the relatively slow hp gas transfer from the pump cell [32] and further reduced during the brief (~1 s) residence time in the lung prior to the application of RF pulses. Despite these polarization losses to relaxation, the spectra still displayed acceptable signal-to-noise ratios of 50–60 depending on SEOP efficiency and possibly individual-to-individual differences in the lungs. Note that the signal from thermally polarized ^{83}Kr could not be observed at all from the lungs.

To qualitatively assess if hp ^{83}Kr reached beyond the finer airways and penetrated into the alveoli without depolarization, the signal from the lungs was compared to that arising from 6 ml of hp krypton mixture in a balloon with no internal structure that had been inflated using the same ventilation system. The ^{83}Kr T_1 inside the balloon exceeded 40 s when fully inflated, so the signal intensity was not substantially affected by relaxation. The signals from lungs were found to be around 30–50% of that observed from the inflated balloon. These intensities are substantially greater than would be expected from ^{83}Kr confined to the anatomical dead space (i.e., the volume of the conducting airways) alone, which typically constitutes less than 5% of the total lung volume [34,35]. Therefore, a substantial fraction of ^{83}Kr lung signal intensity must have originated from the alveolar region.

Fig. 3 shows an MR image (x, y projection with no slice selection) of hp ^{83}Kr in an excised rat lung with 2.3 × 2.3 mm image resolution (raw data) that was obtained from 16 single acquisitions with incremented gradients. The dashed, white line surrounding

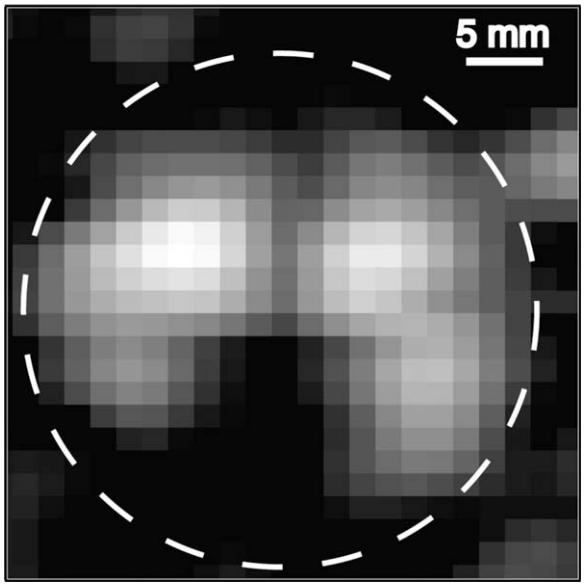

Fig. 3. *Ex vivo* hp ^{83}Kr MR image of a rat lung in the transverse plane. The image was reconstructed from 16 individual SEOP/gas delivery cycles. Each phase encoding step in the x, y lung image was acquired from a single hp ^{83}Kr delivery using no slice selection and resulted in 2.3 × 2.3 mm resolution (raw data). Note that the z-axis is defined as being the direction of the applied magnetic field. The image scale is displayed in the upper right hand corner, and the white, dashed ring indicates the location of the inner wall of the ventilation chamber.

the image indicates the location of the inner wall of the ventilation chamber. Several morphological features are readily observed in the image. The separation between the right and left lung is easily seen, as is a dark area between these two high signal intensity regions. This dark region corresponds to the location of the heart, which contained no hp ^{83}Kr. When the lungs were inflated to 6 ml outside the superconducting magnet, the sides of the lung were observed to touch the inner inflation chamber wall. From the image, it appears that substantial signal intensity extends to the chamber wall and was not merely confined to the major airways.

3.2. Longitudinal relaxation in lungs

Fig. 2b shows a typical hp ^{83}Kr T_1 decay curve in an excised rat lung. The data points are hp ^{83}Kr signal intensities obtained from a series of 24° RF pulses. These relatively long pulses were necessitated by the modest hp ^{83}Kr signal intensity and were found to be a reasonable compromise between obtaining acceptable signal-to-noise ratios and maintaining non-equilibrium polarization long enough to adequately observe T_1 decay. The T_1 values were typically several seconds and were reproducible for a given lung for several hours after excision, but a T_1 range 0.7 to 3.7 s was observed in various lungs (see Table 1). T_1 times in this range should allow *in vivo* hp ^{83}Kr MRI in rats, which breath 1–5 times per second.

Due to of the small gyromagnetic ratio of ^{83}Kr (4% of ^{1}H) compared to ^{3}He (76% of ^{1}H) and ^{129}Xe (28% of ^{1}H), the presence of 20% O_2 was previously found to reduce the ^{83}Kr T_1 time in desiccated canine lung tissue by only 18% from 10.5 to 8.6 s [25]. In comparison, the ^{3}He T_1 time is reduced from hundreds of hours in the absence of paramagnetic species [36,37] to 10–20 s in lungs containing a breathable oxygen mixture [38]. The T_1 of ^{83}Kr was also shown to be much less affected by paramagnetic surface impurities than that of ^{129}Xe [31,32]. Thus, paramagnetic species in the lung will be unlikely to prevent surface sensitive T_1 contrast in hp ^{83}Kr MRI. The small gyromagnetic ratio of ^{83}Kr provides a further advantage for MRI beyond the reduction of paramagnetic relaxation. Due to the low resonance frequency of ^{83}Kr (i.e., 15.4 MHz at 9.4 T) the inductive losses typically found in whole body MRI are expected to be small at any reasonable field strength [39].

Additionally, the T_1 time of hp ^{83}Kr has been shown to increase with increasing surface temperatures presumably due to decreased surface adsorption times [24]. This observation suggests that physiologically relevant temperatures will result in slower relaxation. Longer T_1 times are also to be expected in larger animals due to larger alveoli that presumably lead to decreased surface-to-volume ratios. For instance, the average alveolar diameter is about 225 μm in adult human lungs but only 94 and 58 μm in rats and mice, respectively [40].

Table 1
T_1 data from individual rats[a]

Mass of rats[b] (g)	Hp ^{83}Kr T_1 (s)[c]
245	3.74 ± 0.41
	3.66 ± 0.39
210	2.43 ± 0.13
	2.33 ± 0.20
210	1.55 ± 0.11
193	0.67 ± 0.04
	0.64 ± 0.01
	0.65 ± 0.01

[a] Three lungs were not used for experiments because of damage during transport.
[b] Mass of rat prior to lung excision.
[c] Errors are ± one standard deviation in the residuals resulting from the fit.

3.3. Signal-to-noise in lungs

Like early hp ^{129}Xe lung MRI [6], hp ^{83}Kr MRI will require significant improvements in signal intensity to be biomedically useful. However, isotopically enriched krypton mixtures have yet to be exploited and would immediately improve the observed signal-to-noise ratio by nearly an order of magnitude. Even larger enhancements may be gained from improved ^{83}Kr SEOP that currently generates only about 0.3% spin polarization in a mixture of 95% krypton and 5% nitrogen. Although a higher spin polarization was obtained with more dilute krypton mixtures (i.e., ~1% polarization with 25% krypton mixtures), improved signal intensity was not achieved because of the current lack of a technology that allows for concentrating hp krypton without extensive depolarization.

However, improvement in gas delivery methods [41], better pump cell designs [42], higher laser powers [43], and line-narrowed laser sources [44] have vastly increased the hp ^{3}He and ^{129}Xe NMR signal intensities and production rates. Similar improvements should also advance work with hp ^{83}Kr, and, together with isotopic enrichment, lead to signal enhancements high enough for *in vivo* applications, at least for small animal studies. However, it is important to understand the theoretical limit for spin $I > 1/2$ signal enhancement. At an ambient temperature T and magnetic filed strength B_0 the maximum theoretically possible enhancement factor is

$$f_{\max}^{B_0,T} = \frac{3k_B T}{|\gamma|\hbar B_0(I+1)}, \tag{1}$$

as derived in the Appendix. For ^{83}Kr at 300 K and 9.4 T, the enhancement limit is $f_{\max}^{9.4\ \mathrm{T},300\ \mathrm{K}} = 2.2 \times 10^5$. Thus, the 1200-fold ^{83}Kr signal enhancement currently obtained for 95% krypton mixtures [24] can be further improved by ~180 times before the absolute maximum is reached. Note that for spin $I > 1$ nuclei the signal intensity is not directly proportional to the spin polarization at high polarization values (see Appendix for details).

4. Conclusions

This work demonstrates that hp ^{83}Kr MRI of intact, excised lungs is possible with natural abundance krypton gas. An improvement of up to 180 times the currently obtained signal is theoretically possible, leaving significant room for improvements through the advancement of SEOP technology. An additional increase in the signal-to-noise ratio of almost an order of magnitude is possible using isotopically enriched krypton. The ^{83}Kr T_1 time found in lungs ranged from 0.7 to 3.7 s and should be long enough for *in vivo* work with small animals. The ^{83}Kr T_1 relaxation is expected to be insensitive to the presence of paramagnetic species such as oxygen and therefore capable of providing surface sensitive MRI contrast. Although no attempts have been made to observe a pathology specific contrast in lungs, the experiments presented here are a necessary step in developing hp ^{83}Kr NMR and MRI into useful biomedical tools. Earlier work focused on the T_1 of hp ^{83}Kr but MRI contrast could also be obtained by exploiting T_2 as was done in work with thermally polarized ^{131}Xe ($I = 3/2$) in aerogels [45]. Additional sources of contrast with hp ^{83}Kr may be $T_{1\rho}$, quadrupolar evolution under spin-lock conditions [46,47], and multiple quantum filtering [48–50].

Acknowledgments

The National Science Foundation supported this work under Grants No.: CHE-0135082 and CHE-0719423. The authors wish to thank Michael Olsen and Elden Burk for constructing specialized

glassware and equipment, Professors Fred Salsbury, Randal Basaraba, and Susan Kraft for helpful discussions, and Ramon Saavedra and Markus Seitz for assisting with experiments.

Appendix Hyperpolarization. in spin $I > 1/2$ nuclei

Fully assessing the feasibility of hp ^{83}Kr lung MR requires a discussion of the fundamental limits to hyperpolarization. For the general case of spin $I \geqslant 1/2$ nuclei with a Boltzmann population distribution, it is possible to define a spin polarization, P, as

$$P = \frac{\gamma}{|\gamma|}\frac{\sum_{m=-I}^{I-1}\left(e^{(m+1)\gamma\hbar B_0/k_B T} - e^{m\gamma\hbar B_0/k_B T}\right)}{\sum_{m=-I}^{I} e^{m\gamma\hbar B_0/k_B T}}, \tag{A1}$$

where m represents the z-quantization numbers of the nuclear spin$I$, B_0 is magnetic field strength, γ is the gyromagnetic ratio of the nucleus, and $\gamma/|\gamma|$ accommodates the sign of γ. All of the population terms above other than those of the highest and lowest energy states cancel, and Eq. (A1) simplifies to

$$P = \frac{\gamma}{|\gamma|}\frac{e^{I\gamma\hbar B_0/k_B T} - e^{-I\gamma\hbar B_0/k_B T}}{\sum_{m=-I}^{I} e^{m\gamma\hbar B_0/k_B T}}. \tag{A2}$$

For the thermal equilibrium at high temperatures (i.e., $T \gg |\gamma|\hbar B_0/k_B$), Eq. (A2) further simplifies to

$$P = \frac{2I}{2I+1}\frac{|\gamma|\hbar B_0}{k_B T} \tag{A3}$$

in general and leads to the familiar $P = |\gamma|\hbar B_0/(2k_B T)$ for spin $I = 1/2$ systems. For spin $I > 1/2$ systems, non-Boltzmann population distributions are in principle possible, but the thermal equilibrium (Boltzmann) polarization, P_{tp}, can be calculated through Eq. (A2) at any temperature or Eq. (A3) at high T.

The hyperpolarization, P_{hp}, can be related to P_{tp} by defining an enhancement factor,

$$f_{hp}^{B_0,T} = S_{hp}^{B_0}/S_{tp}^{B_0,T},$$

where $S_{hp}^{B_0}$ is the hp signal measured at the magnetic field strength B_0 and $S_{tp}^{B_0,T}$ is the thermally polarized signal obtained at the same magnetic field and at a temperature T. Defining

$$P_{hp} = P_{tp}^{B_0,T} \cdot f_{hp}^{B_0,T},$$

the previously observed hp ^{83}Kr enhancement of 1200 over the thermal signal obtained for 95% krypton mixtures at 9.4 T and 300 K corresponds to $P_{hp}^{9.4\ T,300\ K} = 0.27\%$. Thus, a further improvement over the currently obtained polarization of more than 350 times is theoretically possible.

However, the concept of polarization is problematic for hp spin $I > 1/2$ systems, which may not possess Boltzmann-like population distributions. For spin $I > 1$ systems, the use of P may also be misleading when discussing the maximum hp signal intensity even if a non-equilibrium, but Boltzmann-like, population distribution is generated. For a general spin I system at any temperature, the signal intensity can be expressed as

$$S = A\frac{\gamma^3}{|\gamma|}B_0\frac{\sum_{m=-I}^{I-1}(C_{I,m'}^{\pm})^2\left(e^{(m+1)\gamma\hbar B_0/k_B T} - e^{m\gamma\hbar B_0/k_B T}\right)}{\sum_{m=-I}^{I} e^{\gamma m\hbar B_0/k_B T}} \tag{A4}$$

with

$$(C_{I,m'}^{\pm})^2 = |\langle I, m' \pm 1|\hat{I}_{\pm}|I, m'\rangle|^2 \tag{A5}$$

being the transition matrix elements obtained using

$$\hat{I}_{\pm}\left|I, m'\right\rangle = \hbar\sqrt{I(I+1) - m'(m'\pm 1)}\left|I, m' \pm 1\right\rangle. \tag{A6}$$

In Eq. (A4), the factor $(C_{I,m'}^{-})^2$ and m′=m+1 are used for spin systems with positive gyromagnetic ratios. For negative gyromagnetic ratios, $(C_{I,m'}^{+})^2$ and m′=m are used. The term A in Eq. (A4) is a constant containing all contributions to the signal intensity other than γ, B_0, and the populations of the various quantum states. In the high temperature limit Eq. (A4) simplifies to

$$S = \frac{2}{3}\frac{A|\gamma^3|\hbar^3 B_0^2}{k_B T}\cdot I(I+1). \tag{A7}$$

Using Eq. (A3) for the polarization at high temperatures, Eq. (A7) can be rewritten as

$$S = A\gamma^2\hbar^2 B_0\frac{(2I+1)(I+1)}{3}P. \tag{A8}$$

However, the relation $S \propto P$ of Eq. (A8) fails at high P (i.e., low spin temperature). Thus, feasibility of hp ^{83}Kr lung MRI is better discussed in relation to the maximum possible thermal signal $S_{tp}^{B_0,T\to 0\ K}$ that would be observed at a given field strength and at 0 K. Thus,

$$S_{tp}^{B_0,T\to 0K} = A\gamma^2\hbar^2 B_0(C_{I,m'=-I}^{\pm})^2 = A\gamma^2\hbar^2 B_0 2I \tag{A9}$$

and the maximum enhancement factor becomes

$$f_{max}^{B_0,T} = S_{tp}^{B_0,T\to 0\ K}/S_{tp}^{B_0,T}. \tag{A10}$$

where $S_{tp}^{B_0,T}$ is the thermal polarization at B_0 and T as described in Eq. (A4) in general and by Eq. (A8) at temperatures $T \gg |\gamma|\hbar B_0/k_B$. Eq. (1) in the main text follows from Eq. (A10) at conditions where Eq. (A8) is valid.

Note that for the simplest case of an $I = 1/2$ system, Eq. (1) in the main text reduces to $f_{max}^{B_0,T} = P^{-1}$ at all temperatures and field strengths. Unlike spin $I = 1/2$ systems, the signal enhancement factors for ^{83}Kr is not directly proportional to the maximum polarization. The maximum polarization enhancement for ^{83}Kr at 9.4T field strength and 300 k is 4.5×10^5 fold, whereas the maximum possible signal enhancement is 2.2×10^5 fold.

References

[1] T.G. Walker, W. Happer, Spin-exchange optical pumping of noble-gas nuclei, Rev. Modern Phys. 69 (1997) 629–642.
[2] T.R. Gentile, G.L. Jones, A.K. Thompson, R.R. Rizi, D.A. Roberts, I.E. Dimitrov, R. Reddy, D.A. Lipson, W. Gefter, M.D. Schnall, J.S. Leigh, Demonstration of a compact compressor for application of metastability-exchange optical pumping of He-3 to human lung imaging, Magn. Reson. Med. 43 (2000) 290–294.
[3] B.M. Goodson, Nuclear magnetic resonance of laser-polarized noble gases in molecules, materials, and organisms, J. Magn. Reson. 155 (2002) 157–216.
[4] A. Cherubini, A. Bifone, Hyperpolarised xenon in biology, Prog. Nucl. Magn. Reson. Spectrosc. 42 (2003) 1–30.
[5] E.J.R. van Beek, J.M. Wild, H.U. Kauczor, W. Schreiber, J.P. Mugler, E.E. de Lange, Functional MRI of the lung using hyperpolarized 3-helium gas, J. Magn. Reson. Imaging 20 (2004) 540–554.
[6] M.S. Albert, G.D. Cates, B. Driehuys, W. Happer, B. Saam, C.S. Springer, A. Wishnia, Biological magnetic-resonance-imaging using laser polarized Xe-129, Nature 370 (1994) 199–201.
[7] H. Middleton, R.D. Black, B. Saam, G.D. Cates, G.P. Cofer, R. Guenther, W. Happer, L.W. Hedlund, G.A. Johnson, M.D. Shattuck, J.C. Schwartz, MR imaging with hyperpolarized ^{3}He gas, Magn. Reson. Med. 33 (1995) 271–275.
[8] Z.Z. Spector, K. Emami, M.C. Fischer, J. Zhu, M. Ishii, J. Yu, S. Kadlecek, B. Driehuys, R.A. Panettieri, D.A. Lipson, W. Gefter, J. Shrager, R.R. Rizi, A small animal model of regional alveolar ventilation using (HPHe)-He-3 MRI, Acad. Radiol. 11 (2004) 1171–1179.
[9] J.C. Woods, C.K. Choong, D.A. Yablonskiy, J. Bentley, J. Wong, J.A. Pierce, J.D. Cooper, P.T. Macklem, M.S. Conradi, J.C. Hogg, Hyperpolarized He-3 diffusion MRI and histology in pulmonary emphysema, Magn. Reson. Med. 56 (2006) 1293–1300.
[10] T.A. Altes, J. Mata, E.E. de Lange, J.R. Brookeman, J.P. Mugler, Assessment of lung development using hyperpolarized helium-3 diffusion MR imaging, J. Magn. Reson. Imaging 24 (2006) 1277–1283.
[11] M.C. Fischer, S. Kadlecek, J.S. Yu, M. Ishii, K. Emami, V. Vahdat, D.A. Lipson, R.R. Rizi, Measurements of regional alveolar oxygen pressure using hyperpolarized He-3 MRI, Acad. Radiol. 12 (2005) 1430–1439.
[12] R.W. Mair, M.I. Hrovat, S. Patz, M.S. Rosen, I.C. Ruset, G.P. Topulos, L.L. Tsai, J.P. Butler, F.W. Hersman, R.L. Walsworth, He-3 lung imaging in an open access, very-low-field human magnetic resonance imaging system, Magn. Reson. Med. 53 (2005) 745–749.

[13] K. Ruppert, J.R. Brookeman, K.D. Hagspiel, J.P. Mugler, Probing lung physiology with xenon polarization transfer contrast (XTC), Magn. Reson. Med. 44 (2000) 349–357.
[14] K. Ruppert, J.F. Mata, J.R. Brookeman, K.D. Hagspiel, J.P. Mugler, Exploring lung function with hyperpolarized Xe-129 nuclear magnetic resonance, Magn. Reson. Med. 51 (2004) 676–687.
[15] B. Driehuys, G.P. Cofer, J. Pollaro, J.B. Mackel, L.W. Hedlund, G.A. Johnson, Imaging alveolar-capillary gas transfer using hyperpolarized Xe-129 MRI, Proc. Natl. Acad. Sci. USA 103 (2006) 18278–18283.
[16] J. Kershaw, K. Nakamura, Y. Kondoh, A. Wakai, N. Suzuki, I. Kanno, Confirming the existence of five peaks in Xe-129 rat head spectra, Magn. Reson. Med. 57 (2007) 791–797.
[17] C. Hilty, T.J. Lowery, D.E. Wemmer, A. Pines, Spectrally resolved magnetic resonance imaging of a xenon biosensor, Angew. Chem. Int. Ed. 45 (2006) 70–73.
[18] L. Schroder, T.J. Lowery, C. Hilty, D.E. Wemmer, A. Pines, Molecular imaging using a targeted magnetic resonance hyperpolarized biosensor, Science 314 (2006) 446–449.
[19] D.O. Kuethe, A. Caprihan, E. Fukushima, R.A. Waggoner, Imaging lungs using inert fluorinated gases, Magn. Reson. Med. 39 (1998) 85–88.
[20] R.E. Jacob, Y.V. Chang, C.K. Choong, A. Bierhals, D.Z. Hu, J. Zheng, D.A. Yablonskiy, J.C. Woods, D.S. Gierada, M.S. Conradi, F-19 MR imaging of ventilation and diffusion in excised lungs, Magn. Reson. Med. 54 (2005) 577–585.
[21] J.E. Repine, Scientific perspectives on adult respiratory-distress syndrome, Lancet 339 (1992) 466–469.
[22] R.R. Baker, M. Dixon, The retention of tobacco smoke constituents in the human respiratory tract, Inhal. Toxicol. 18 (2006) 255–294.
[23] B. Fubini, C.O. Arean, Chemical aspects of the toxicity of inhaled mineral dusts, Chem. Soc. Rev. 28 (1999) 373–381.
[24] Z.I. Cleveland, G.E. Pavlovskaya, K.F. Stupic, C.F. LeNoir, T. Meersmann, Exploring hyperpolarized ^{83}Kr by remotely detected NMR relaxometry, J. Chem. Phys. 124 (2006) 044312.
[25] G.E. Pavlovskaya, Z.I. Cleveland, K.F. Stupic, T. Meersmann, Hyperpolarized krypton-83 as a new contrast agent for magnetic resonance imaging, Proc. Natl. Acad. Sci. USA 102 (2005) 18275–18279.
[26] S.R. Schaefer, G.D. Cates, W. Happer, Determination of spin-exchange parameters between optically pumped rubidium and Kr-83, Phys. Rev. A 41 (1990) 6063–6070.
[27] R. Butscher, G. Wäckerle, M. Mehring, Nuclear quadrupole surface interaction of gas phase ^{83}Kr: comparison with ^{131}Xe, Chem. Phys. Lett. 249 (1996) 444–450.
[28] D. Brinkmann, D. Kuhn, Nuclear magnetic-relaxation of Kr-83 in krypton gas, Phys. Rev. A 21 (1980) 163–167.
[29] Z.I. Cleveland, T. Meersmann, Density independent contributions to longitudinal relaxation in ^{83}Kr, ChemPhysChem 9 (2008) 1375–1379.
[30] K.F. Stupic, Z.I. Cleveland, G.E. Pavlovskaya, T. Meersmann, Quadrupolar relaxation of hyperpolarized krypton-83 as a probe for surfaces, Solid State Nucl. Magn. Reson. 29 (2006) 79–84.
[31] Z.I. Cleveland, G.E. Pavlovskaya, K.F. Stupic, J.B. Wooten, J.E. Repine, T. Meersmann, Detection of tobacco smoke deposition by hyperpolarized krypton-83 MRI, Magn. Reson. Imaging 26 (2008) 270–278.
[32] Z.I. Cleveland, K.F. Stupic, G.E. Pavlovskaya, J.E. Repine, J.B. Wooten, T. Meersmann, Hyperpolarized ^{83}Kr and ^{129}Xe NMR relaxation measurements of hydrated surfaces: implications for materials science and pulmonary diagnostics, J. Am. Chem. Soc. 129 (2007) 1784–1792.
[33] L. Zhao, R. Mulkern, C.H. Tseng, D. Williamson, S. Patz, R. Kraft, R.L. Walsworth, F.A. Jolesz, M.S. Albert, Gradient-echo imaging considerations for hyperpolarized Xe-129 MR, J. Magn. Reson. Ser. B 113 (1996) 179–183.
[34] W.S. Fowler, Lung function studies. 2. The respiratory dead space, Am. J. Physiol. 154 (1948) 405–416.
[35] H. Heller, M. Konen-Bergmann, K.D. Schuster, An algebraic solution to dead space determination according to Fowler's graphical method, Comput. Biomed. Res. 32 (1999) 161–167.
[36] M.F. Hsu, G.D. Cates, I. Kominis, I.A. Aksay, D.M. Dabbs, Sol–gel coated glass cells for spin-exchange polarized He-3, Appl. Phys. Lett. 77 (2000) 2069–2071.
[37] E. Babcock, B. Chann, T.G. Walker, W.C. Chen, T.R. Gentile, Limits to the polarization for spin-exchange optical pumping of He-3, Phys. Rev. Lett. 96 (2006) 083003.
[38] H.E. Moller, X.J. Chen, B. Saam, K.D. Hagspiel, G.A. Johnson, T.A. Altes, E.E. de Lange, H.U. Kauczor, MRI of the lungs using hyperpolarized noble gases, Magn. Reson. Med. 47 (2002) 1029–1051.
[39] D.I. Hoult, C.N. Chen, V.J. Sank, The field-dependence of NMR imaging. 2. Arguments concerning an optimal field-strength, Magn. Reson. Med. 3 (1986) 730–746.
[40] R.R. Mercer, M.L. Russell, J.D. Crapo, Alveolar septal structure in different species, J. Appl. Physiol. 77 (1994) 1060–1066.
[41] K. Knagge, J. Prange, D. Raftery, A continuously recirculating optical pumping apparatus for high xenon polarization and surface NMR studies, Chem. Phys. Lett. 397 (2004) 11–16.
[42] I.C. Ruset, S. Ketel, F.W. Hersman, Optical pumping system design for large production of hyperpolarized Xe-129, Phys. Rev. Lett. 96 (2006) 053002.
[43] A.L. Zook, B.B. Adhyaru, C.R. Bowers, High capacity production of >65% spin polarized xenon-129 for NMR spectroscopy and imaging, J. Magn. Reson. 159 (2002) 175–182.
[44] J.N. Zerger, M.J. Lim, K.P. Coulter, T.E. Chupp, Polarization of Xe-129 with high power external-cavity laser diode arrays, Appl. Phys. Lett. 76 (2000) 1798–1800.
[45] G. Pavlovskaya, A.K. Blue, S.J. Gibbs, M. Haake, F. Cros, L. Malier, T. Meersmann, Xenon-131 surface sensitive imaging of aerogels in liquid xenon near the critical point, J. Magn. Reson. 137 (1999) 258–264.
[46] I. Hancu, J.R.C. van der Maarel, F.E. Boada, Detection of sodium ions in anisotropic environments through spin-lock NMR, Magn. Reson. Med. 47 (2002) 68–74.
[47] J.R.C. van der Maarel, Thermal relaxation and coherence dynamics of spin 3/2. II. Strong radio-frequency field, Concepts Magn. Reson. A 19A (2003) 117–133.
[48] G. Jaccard, S. Wimperis, G. Bodenhausen, Multiple quantum NMR spectroscopy of $S = 3/2$ spins in isotropic phase: a new probe for multiexponential relaxation, J. Chem. Phys. 85 (1986) 6282–6293.
[49] T. Meersmann, S.A. Smith, G. Bodenhausen, Multiple-quantum filtered xenon-131 NMR as a surface probe, Phys. Rev. Lett. 80 (1998) 1398–1401.
[50] T. Meersmann, M. Deschamps, G. Bodenhausen, Probing aerogels by multiple quantum filtered Xe-131 NMR spectroscopy, J. Am. Chem. Soc. 123 (2001) 941–945.